ACS APPLIED MATERIALS & INTERFACES

www.acsami.org

Research Article

An Innovative Nanobody-Based Electrochemical Immunosensor Using Decorated Nylon Nanofibers for Point-of-Care Monitoring of Human Exposure to Pyrethroid Insecticides

Ahmed Y. El-Moghazy,* Jingqian Huo, Noha Amaly, Natalia Vasylieva, Bruce D. Hammock, and Gang Sun*

Cite This: *ACS Appl. Mater. Interfaces* 2020, 12, 6159–6168

Read Online

ACCESS | Metrics & More | Article Recommendations | Supporting Information

ABSTRACT: A novel ultrasensitive nanobody-based electrochemical immunoassay was prepared for assessing human exposure to pyrethroid insecticides. 3-Phenoxybenzoic acid (3-PBA) is a common human urinary metabolite for numerous pyrethroids, which broadly served as a biomarker for following the human exposure to this pesticide group. The 3-PBA detection was via a direct competition for binding to alkaline phosphatase-embedded nanobodies between free 3-PBA and a 3-PBA-bovine serum albumin conjugate covalently immobilized onto citric acid-decorated nylon nanofibers, which were incorporated on a screen-printed electrode (SPE). Electrochemical impedance spectroscopy (EIS) was utilized to support the advantage of the employment of nanofibrous membranes and the success of the immunosensor assembly. The coupling between the nanofiber and nanobody technologies provided an ultrasensitive and selective immunosensor for 3-PBA detection in the range of 0.8 to 1000 pg mL^{-1} with a detection limit of 0.64 pg mL^{-1}. Moreover, when the test for 3-PBA was applied to real samples, the established immunosensor proved to be a viable alternative to the conventional methods for 3-PBA detection in human urine even without sample cleanup. It showed excellent properties and stability over time.

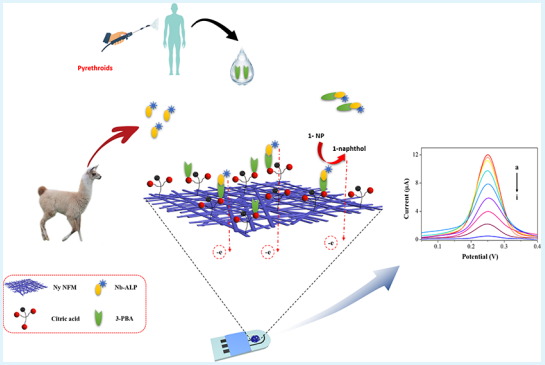

KEYWORDS: *nylon, nanofibers, electrochemical immunosensor, nanobody, pyrethroids, point-of-care, 3-PBA*

1. INTRODUCTION

Nanofibers (NFs) and nanofibrous membranes (NFMs) produced via electrospinning are promising materials, due to their ultrahigh specific surface areas, and have received a growing interest for their applications in many fields including environmental,[1−3] energy,[4,5] medical,[6−8] and food applications.[1,9] One of the aspects on which biosensor performance depends is the sensor matrix material. An appropriate matrix provides high loading capacity for biorecognition elements and accessibility of target analytes to the active sites. As a result, the employment of the nanofibers with the high surface areas and microporous network in the development of the sensors has produced higher sensitivity and lower limits of detection (LOD) to toxicants.[9,10] Polycaprolactam (nylon 6) fibers, commonly known as polyamide fibers, have been commonly served as media supporting materials, owing to their desired chemical stability and biocompatibility as well as notable mechanical properties.[11] However, compared with other polymers such as polyvinyl alcohol and cellulose, polyamide lacks reactive groups for chemical modifications and biomolecule immobilization. Polyamide fibers incorporated with desired reactive groups are ideal media for various applications such as protein immobilization.[12]

Pyrethroids are widely used synthetic insecticides for agricultural and private household uses as an alternative to organophosphate insecticides.[13,14] The impacts of exceptionally high pyrethroid exposure include many harmful effects. Moreover, long-term exposure to high levels of these synthetic insecticides may contribute to developmental neurotoxicity,[15] harmful impacts on male reproduction,[16] and endocrine system disruption.[17]

3-Phenoxybenzoic acid (3-PBA) is the most known metabolite from hydrolysis of numerous pyrethroid pesticides.[18−20] These pyrethroids in mammals are hydrolyzed by esterases to 3-phenoxybenzyl alcohol or 3-phenoxybenzaldehyde, which rapidly turned into 3-PBA. Hence, 3-PBA is widely employed as the common biomarker for human pyrethroid exposure,[19,21] although it has other uses as well.

Using 3-PBA in the analysis of pyrethroid metabolite have been reported[22−27] with high sensitivity and accuracy in

Received: September 7, 2019
Accepted: January 13, 2020
Published: January 13, 2020

https://dx.doi.org/10.1021/acsami.9b16193
ACS Appl. Mater. Interfaces 2020, 12, 6159–6168

Scheme 1. Modification of Nylon NFM with Citric Acid

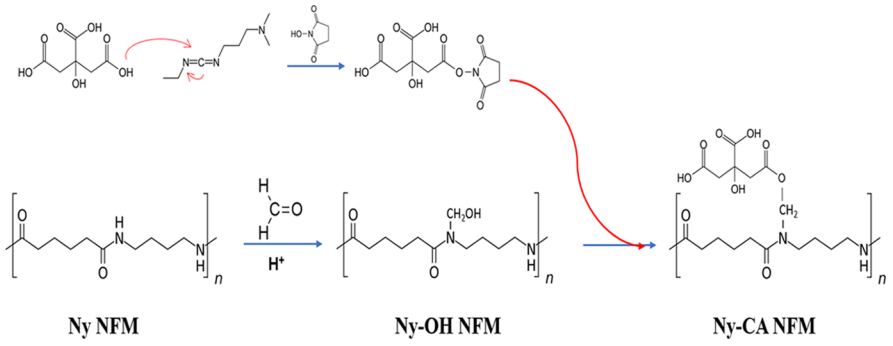

different real samples. However, they are not convenient and practical for field sensing and monitoring applications and require expensive instruments, highly trained people, and transport to a central laboratory. Despite the tremendous popularity of ELISA, the feasibility of it as a point-of-care monitoring tool is hard to realize.

Electrochemical biosensors are commonly assembled for point-of-care applications owing to their unique merits such as rapid real-time detection and the operational procedures for on-site analysis application. Electrochemical immunosensing systems are receiving an expanding attention due to the operational simplicity, high sensitivity, and high selectivity toward the desired target, depending on the specific antibody−antigen interaction on the electrode surface.[28] Nevertheless, the instability of recombinant antibodies requires a very careful fabrication and application processes.

Nanobodies (Nbs), termed variable heavy chain (VHH) domains or single-domain antigen-binding fragments, are derived from heavy-chain-only antibodies that occur naturally in the serum of camelids.[29] Several advantages the Nbs could afford over the traditional antibodies such as small size and ease of expression, more thermal and chemical stability, high solubility, suitability for the determination of small molecules (MW < 1500 Da) in different matrices, proteolysis resistance, and ease of genetic manipulation[30,31] as well as the intact and unique antigen-binding antibody fragments.[30] However, research on use of the Nbs in electrochemical sensors is still limited.

Herein, we adapted and integrated different technologies, including nanofibrous materials, nanobodies, and electrochemical methods to develop a novel sensitive electrochemical competitive immunosensor for rapid assaying of 3-PBA. The nanosensor is assembled based on the use of novel nylon nanofibrous membranes that were surface-modified with citric acid (CA) and a nanobody−alkaline phosphatase (Nb-ALP) fusion protein. The proposed immunosensor was fabricated by immobilization of 3-PBA onto the surface of the CA and Nb-ALP-decorated nylon nanofibrous membrane and then incorporation of the membrane onto a screen-printed electrode (SPE). Differential pulse voltammetry (DPV) was used to determine the activity of the alkaline phosphatase.

2. CHEMICALS, MATERIALS, AND INSTRUMENTS

Polycaprolactam (nylon 6, Ny), formaldehyde, formic acid, citric acid (CA), 3-phenoxybenzoic acid and its analogues, permethrin, cypermethrin, deltamethrin, fenpropathrin, phenothrin, ethanolamine (EA), 1-naphthyl phosphate (1-NP), and *p*-nitrophenyl phosphate (pNPP) were supplied by Sigma (St. Louis, MO) and used as received. *N*-Ethyl-*N*′-(3- dimethyl aminopropyl) carbodiimide hydrochloride (EDC), *N*-hydroxyl succinimide (NHS), disodium hydrogen phosphate (Na_2HPO_4), monosodium orthophosphate (NaH_2PO_4), and *O*-phosphoric acid (85%) were purchased from Acros Chemical (Pittsburgh, PA, USA). All other chemicals were of analytical grade and were supplied by Merck (Darmstadt, Germany).

A 263A potentiostat/galvanostat equipped with a frequency response detector (FRD100) (Princeton Applied Research Co., Oak Ridge, TN, USA) was used for the electrochemical measurements. The disposable SPE, comprising a carbon working electrode, a carbon counter electrode, and an Ag/AgCl reference electrode, was purchased from eDAQ Inc. (Colorado, US). The morphological characterizations of the polymeric nanofibrous membranes were implemented by a FEI 430 Nova NanoSEM scanning electron microscope (SEM).

The FT-IR spectra of membrane materials were achieved by using a Nicolet 6700 spectrometer, followed by the pressing of the grounded Ny NFMs at different reaction steps with anhydrous KBr; FT-IR spectra of these specimens were scanned in the wavenumber range of 500−4000 cm^{-1} with a resolution of 4 cm^{-1}.

2.1. Fabrication of Nylon 6 Nanofibrous Membranes (Ny NFM). A formic acid solution of nylon 6 (15% w/v) was prepared by mechanical stirring at 60 °C for 8 h. Electrospinning was carried out using a 10 mL plastic syringe with an 18-gauge tubular metal needle with a flat tip. The nylon nanofibrous membranes were fabricated through electrospinning of the nylon solution at room temperature utilizing a DXES-1 spinning equipment supplied with an applied voltage of 20 kV and spinning rate of 0.7 mL/h with a 23 cm needle tip far from the collector surface. The resultant nylon nanofibrous membranes (Ny NFM) were kept for 12 h in a vacuum oven at 40 °C for drying. The nylon solution (15% w/v) was used to cast a thin membrane film (Ny-CM) in similar thickness to the Ny NFM. A 4 mm Ny NFM disc with 0.05 mm thickness was laminated on the working electrode of the SPE using a conductive paste to fabricate Ny NFM/SPE, and similarly, an Ny-CM/SPE was prepared in parallel by using an Ny-CM disc.

2.2. Chemical Modifications of Nylon Nanofibrous Membranes. Ny NFMs were chemically modified according to reactions shown in Scheme 1. First, nylon 6 NFMs were turned to *N*-methylol nylon 6 by converting the amide (N−H) groups to *N*-methylol groups via reacting with formaldehyde, and the product was designated as Ny-OH NFMs.[32,33] Briefly, 2 g of Ny NFM was immersed in 25 mL formaldehyde (36.5% w/v) and 0.2 mL phosphoric acid (85% w/w) at a temperature of 60 °C for about 1 h. Then, the prepared Ny-OH NFMs were washed several times with distilled water.

The hydroxyl groups on the Ny-OH NFMs were then reacted with the carboxylic groups of citric acid (CA) in a procedure performed as follows:[3] a CA solution 8% (w/v) was prepared via dissolving CA in 10 mL of PBS buffer pH 7.2, synchronously, EDC and NHS were added into the CA solution at a final concentration of 1 mM. This blend was energetically mixed at room temperature for 2 h. Afterward, the as-prepared Ny-OH NFMs were dipped into the CA/EDC/NHS solution for 60 min at 60 °C. Subsequently, the resulted membranes

https://dx.doi.org/10.1021/acsami.9b16193
ACS Appl. Mater. Interfaces 2020, 12, 6159−6168

Scheme 2. Fabrication Process and Sensing Mechanism of Nanobody-Based Electrochemical Immunosensor for 3-PBA Detection

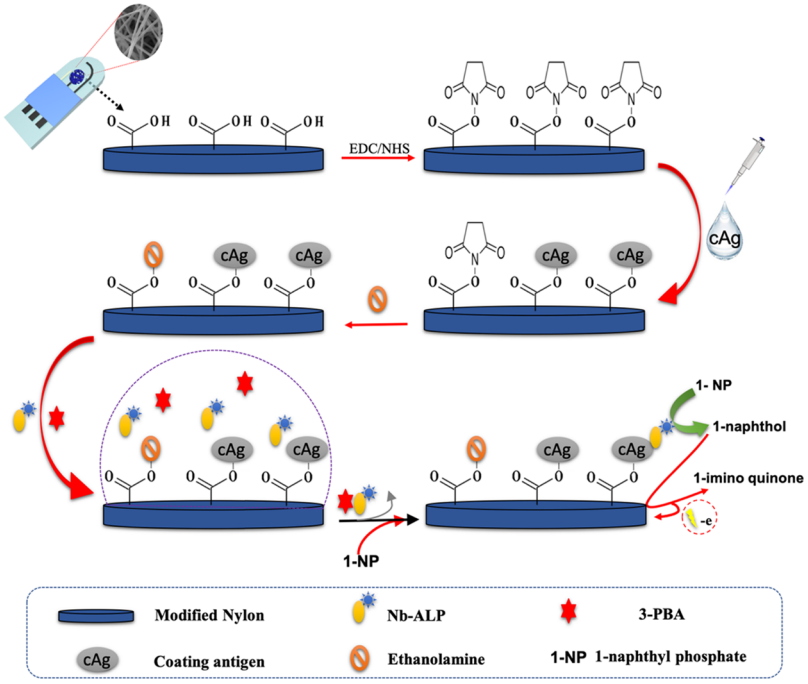

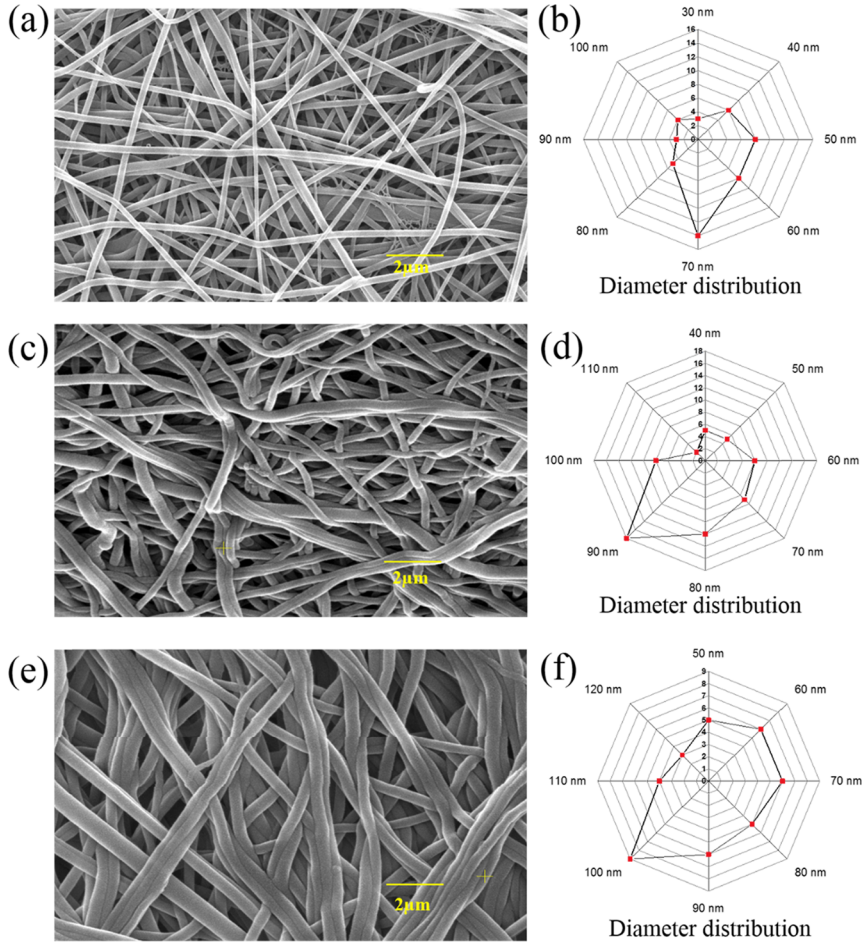

Figure 1. SEM images of (a) pristine nylon NFM, (c) Ny-OH NFM, and (e) Ny-CA. Fiber diameter distributions of (b) nylon NFM, (d) Ny-OH NFM, and (f) Ny-CA.

https://dx.doi.org/10.1021/acsami.9b16193
ACS Appl. Mater. Interfaces 2020, 12, 6159−6168

(Ny-CA NFM) were washed by PBS and dried in a vacuum oven at 80 °C for 1 h.

2.3. Production of Anti-3-PBA Nb-ALP Fusion Protein. The Nb-ALP fusion protein with a 6× His tag at its C-terminal end was created as depicted previously.[34] Briefly, primers were used to amplify the Nb gene (forward primer: GAG GAG GAG GTG GCC CAG CCG GCC CAG GTG CAG CTC GTG GAG TCT GGG GGA, reverse primer: GAG GAG GAG CTG GCC CCC GAG GCC GCG TCT TGT GGT TTT GGT GTC TTG GG). After a ligation reaction, the ligation products were then transformed into chemically competent cells of *E. coli* strain BL21(DE3) pLysS, then the positive clones grown on the plates were picked up for sequencing, and this was followed by multiplication, induction, and purification of the crude fusion protein by affinity chromatography using a high-capacity nickel-immobilized metal-ion-resin column. The elution of the purified Nb-ALP fusion protein was carried out with an elution buffer (PBS containing 100 mM imidazole) subsequently by the dialysis with PBS at 4 °C for 72 h to obtain the Nb-ALP fusion protein and stored at −20 °C to use.

2.4. Fabrication of the Immunosensor. First, the carboxylic groups of the Ny-CA NFM/SPE were activated by incubation with 100 μL of 1 mM EDC/NHS for 1 h. After being rinsed with PBS, 6 μL 3-phenoxybenzoic acid/bovine serum albumin conjugate (3PBA-BSA) prepared according to Shan et al.[35] at a concentration of 10 μg/mL in PBS was dropped onto the surface of EDC/NHS=-decorated Ny-CA NFM/SPE for 2 h at 4 °C. Followed by the washing with PBS to remove any unimmobilized antigen, the remaining active groups were blocked with 100 μL of 2% ethanolamine (EA) at room temperature for 1 h and then rinsed again with PBS and stored at 4 °C to use.

The competition step was performed by incubating 50 μL of Nb-ALP (400 μg mL^{-1}) and equivalent volume from different concentrations of 3-PBA on the immunosensor surface for 40 min at room temperature. In the wake of washing multiple times by PBST (PBS containing 0.5% Tween 20), the ALP activity was measured electrochemically using differential pulse voltammetry (DPV). The assembly steps of the 3-PBA nanosensor and detection mechanism are illustrated in the following schematic diagram (Scheme 2).

2.5. Electrochemical Measurements. Electrochemical impedance spectroscopy (EIS) was used for characterizing of the immunosensor surface using ferri/ferrocyanide ($[Fe(CN)_6]^{4-/3-}$) dissolved in PBS at a concentration of 2.5 mM. The Nyquist plots were recorded at an applied potential of 0.09 V versus Ag/AgCl, with a frequency range from 10 KHz to 1 Hz. DPV measurements were carried out with an applied potential range of 0−400 mV, pulse amplitude of 60 mV, pulse period of 200 ms, pulse width of 100 ms, and scan rate of 50 mV/s. The signal generation depends on ALP dephosphorylates of non-electroactive 1-NP to 1-naphthol, which electrochemically oxidized to 1-iminoquinone on the electrode surface.

2.6. Applicability of the Nanosensor for Real Sample Analysis. Urine samples were gathered from a healthy person and spiked with various concentrations of 3-BPA from 0.01 to 0.5 ng mL^{-1} after the negative 3-PBA content was verified using LC−MS. The resulting samples were then diluted 10 times with PBS followed by direct analysis using the assembled nanobody-based sensor.

3. RESULTS AND DISCUSSION

3.1. Morphologies and Structure. The nanosensor was designed based on the use of a chemically modified nylon nanofibrous membrane as a supporting matrix with immobilized antigen to satisfy the following important principles: (i) the hydrophilicity of the matrix that improves the performance of the sensor in aqueous samples, (ii) the physical and chemical characteristics of nylon as a robust matrix for the fabrication and detection processes, and (iii) the ultrahigh surface and microporous areas that can increase the efficiency and the accessibility of the active sites to the targets.

The morphologies of the nylon NFMs during the different steps of chemical modifications were characterized by scanning electron microscopy (SEM). As shown in Figure 1a,b, the nylon NFMs revealed randomly oriented three-dimensional nonwoven membrane structures with an average fiber diameter of 75 nm. The average diameter of the nanofiber increased to 90 nm after the reaction with formaldehyde in an acidic medium (Figure 1c,d). Consequently, the nanofiber diameter was further increased to 100−110 nm after incorporation of CA, as illustrated in Figure 1e,f. The increase of the nanofiber diameters after the modifications were possibly due to increased hydrophilicity and swelling behavior of the methylolated and carboxylated nylon fibers and the impregnations of the fibers with different aqueous solutions through the modifications.[36] This observation agreed well with the water wetting properties of the nylon NFMs before and after the modification where the contact angle measurements (Figure S2) decreased from 85° for the nonmodified nylon NFM to 52° for the CA grafted Ny NFM during a contact time of 30 s, attributing to the presence of hydroxyl and carboxyl groups after the modifications by formaldehyde and citric acid, respectively.

FT-IR spectroscopy was utilized to characterize successful grafting of CA onto the NFM. FT-IR spectra of the pristine nylon nanofibers before and after modifications are shown in Figure 2. The conversion of the amide groups of nylon to

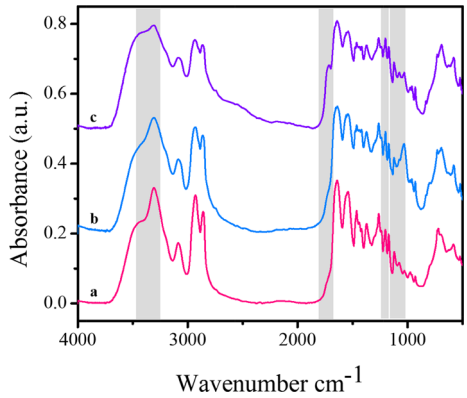

Figure 2. FT-IR spectra of (a) pristine Ny NFM, (b) *N*-methylol Ny NFM, and (c) Ny NFM grafted with citric acid.

hydroxyl groups by formaldehyde was confirmed by the appearance of a new peak at 1042 cm^{-1} for the C−O of primary alcohol, broadening the band in the region 3250−3500 cm^{-1}, corresponding to the stretching mode of formed hydroxyl groups on the surface of the nylon NFM. Also, a relatively weak decrease in the intensity of C═O and N−H of amide peaks at 1630 cm^{-1} and 1552 cm^{-1}, respectively, can be the evidence of the reaction on the N−H group in the nylon.

The appeared peak of C═O of the ester at 1750 cm confirmed the effective incorporation of carboxyl groups onto the nylon NFM surface between the methylene hydroxy (CH_2OH) on the nylon and carboxylic acid (−COOH) group of CA,[3,37] and the decrease of hydroxyl group peak intensity at 1042 cm^{-1}. With increase of the initial CA concentration, the intensity of the new peak at 1750 cm^{-1} of the resulting ester was increased correspondingly. The same trend in intensity change was observed at 1040 cm^{-1} (Figure S1).

3.2. Electrochemical Characterization. EIS is a suitable tool for studying the surface features of the different modified

https://dx.doi.org/10.1021/acsami.9b16193
ACS Appl. Mater. Interfaces 2020, 12, 6159−6168

electrodes through assembling and dynamic performances of electrochemical processes.[38] Herein, the EIS was used to study the advantages of the nanofibrous membranes and to validate the sensors fabricated through these steps. The most common equivalent circuit, which was used in the electrochemical immunosensors development, is provided by Randles.[39−41] As shown in Figure 3A (inset), the components of the circuit are

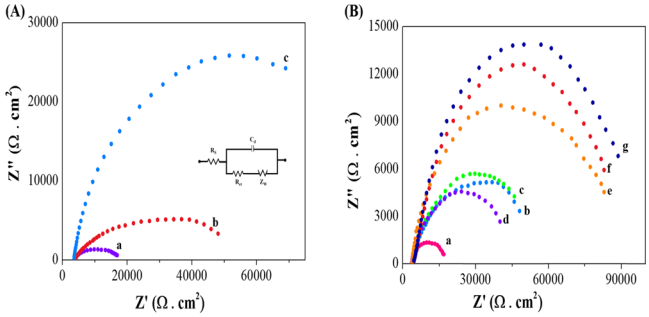

Figure 3. Electrochemical impedance spectroscopies in 2.5 mM $[Fe(CN)_6]^{4-/3-}$ for (A) bare SPE (a), Ny NFM/SPE (b), and Ny-CM/SPE (c) (inset: Randles model for the common equivalent circuit). (B) Assembling steps of the 3-PBA immunosensor: bare SPE (a), Ny NFM/SPE (b), Ny-CA NFM/SPE (c), activated Ny-CA NFM/SPE (d), 3PBA-BSA/ Ny-CA NFM/SPE (e), EA/3PBA-BSA/ Ny-CA NFM/SPE (f), and Nb-ALP/ EA/3PBA-BSA/Ny-CA NFM/SPE (g).

the electrolyte resistance (R_s), the electron-transfer resistance (R_{et}), capacitance of the double layer (C_d), and Warburg impedance (Z_w) where R_s and Z_w represent the resistance of the supporting electrolyte and the diffusion properties of the redox probe in the solution, respectively, and are not affected by the occurred modifications on the electrode surface. The Nyquist plot contains two parts. At higher frequencies, a semicircle portion reflects R_{et} of the surface of the electrode, which is the most important parameter, and its value changed due to the modification and interaction of the electrode surface with the electrolyte. The second part at the lower frequencies is a linear portion, which presents the diffusion-limited process.[42] As shown in Figure 3A, the Nyquist plot of the bare SPE reveals a very low resistance value (curve a). The modification of SPE with the casted nylon membrane (Ny-CM) exhibited a dramatic increase in the resistance of the electron transfer due to the insulation of the electrode surface by the Ny-CM (curve b). While with the replacement of the casted membrane by the nanofibrous membrane (Ny NFM) with its distinctive porous structure decreased the R_{et} by more than five times (curve c), it facilitates the access of $[Fe(CN)_6]^{4-/3-}$ and accelerates the electron transfer toward the electrode surface, making this unique material to be introduced as an ideal matrix for fabricating highly sensitive sensing systems.

The fabrication of the nanosensor was finalized by the application of the chemically modified nanofibers (Ny-CA) with EDC/NHS as a supported matrix for immobilization of 3PBA-BSA. Figure 3B confirmed the success of the fabrication steps. The bare SPE showed very low electron-transfer resistance (curve a). After the lamination of the electrode surface with the nylon nanofibrous membranes, the semicircle increased, revealing that the nanofibrous membranes acted as an electron transfer barrier (curve b). The grafting of CA onto the Ny NFM enhanced the hydrophilicity (Figure S2) but induced a small increase of the R_{et} (curve c), which could be ascribed to the electrostatic repulsion between the same negative charge of $[Fe(CN)_6]^{3-/4-}$ and carboxylic groups of the CA. The activation of the modified nylon nanofibrous membranes with EDC/NHS induced a decrease of R_{et} (curve d), possibly owing to the replacement of the carboxyl group by NHS groups, which facilitates the electrolyte move through the porous structure of the nanofibrous membranes. The deterred electron transfer continued with immobilization of 3PBA-BSA, blocking of the unreacted sites and reaction with Nb-ALP (curves e−g), and evidence of the effective immobilization of blocking groups. All the EIS results confirmed the successful assembly of the nanosensor.

3.3. Experimental Parameter Optimization. In order to accomplish the most effective analytical performance of the fabricated immunosensor for 3-PBA detection, different important experimental conditions were optimized by measuring the achieved currents using DPV, which include 3PBA-BSA concentration, required time for immobilization of 3PBA-BSA, Nb-ALP concentration, the immunoreaction time, substrate concentration, and the blocking process.

3.3.1. Antigen Concentration. The 3PBA-BSA concentration was optimized using the reaction with the Ny-CA NFM/SPE, an incubation time of 2 h, an Nb-ALP concentration of 400 μg mL^{-1}, a substrate concentration of 1 mg mL^{-1}, and an immunoreaction time of 40 min. As shown in Figure 4a, the current response increased gradually with the increment of the 3PBA-BSA concentration, and the maximum response at a concentration of 10 μg mL^{-1} was observed. Nevertheless, the higher concentrations than 10 μg mL^{-1} prompted a decline in the current achieved. This may be due to the steric hindrance of the membrane that could obstruct the ability of nanobodies to reach the binding sites on the nanofibers surfaces and the moving of the electrons from the analyte solution toward the electrode surface.

3.3.2. Antigen Immobilization Time. The necessary time for the 3PBA-BSA immobilization on the Ny-CA NFM/SPE was adjusted at a 3PBA-BSA concentration of 10 μg mL^{-1}, Nb-ALP concentration of 400 μg mL^{-1}, substrate concentration of 1 mg mL^{-1}, and immunoreaction time of 40 min. As seen in Figure 4b, expanding of the immobilization time of the Ny-CA NFM/SPE with 3PBA-BSA from 30 up to 120 min resulted in an increase of the current response and achieved a plateau at the incubation time over 120 min, revealing the saturation of the immobilization sites of the nanofibrous membrane. A tethering time of 120 min was selected for the further experiments.

3.3.3. Nanobody Concentration. The nanobody concentration is considered as a key factor in the development of the sensitive competitive immunoassays as the increase of the nanobody concentration decreases the sensitivity of the immunosensor, and lower nanobody concentrations reduce the signal response. For the optimization of the nanobody concentration, the fabricated immunosensor immobilized with 10 μg mL^{-1} 3PBA-BSA for 120 min was incubated with different Nb-ALP concentrations in a range of 100 to 600 μg mL^{-1} for 40 min. The current responses were recorded at a substrate concentration of 1 mg mL^{-1}. As observed in Figure 4c, the signal response was directly proportional to the Nb-ALP concentration, and until a concentration of 400 μg mL^{-1}, the increase in the generated current was achieved, which was selected for the electrochemical assays.

https://dx.doi.org/10.1021/acsami.9b16193
ACS Appl. Mater. Interfaces 2020, 12, 6159−6168

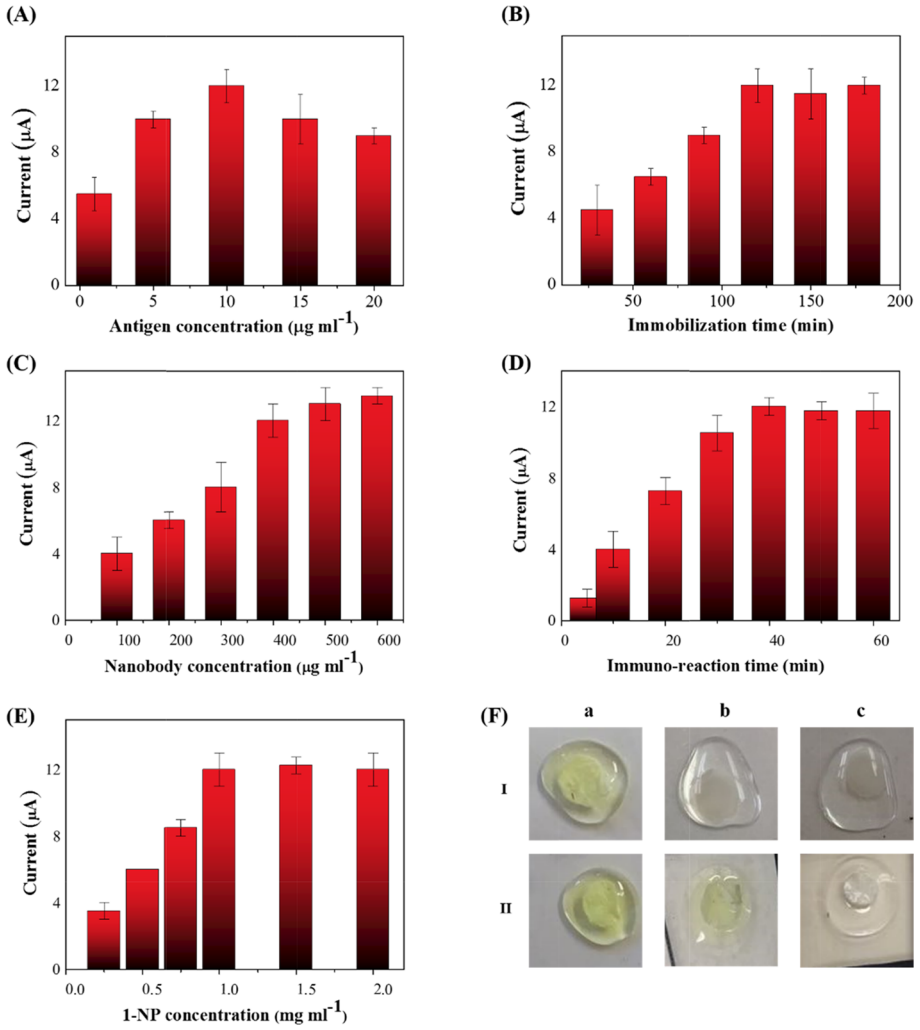

Figure 4. Dependences of the obtained currents via DPV on (A) antigen concentration, (B) antigen immobilization time, (C) nanobody concentration, (D) immunoreaction time, and (E) 1-NP concentration. (F) Blocking process of the active sites of (I) Ny-CM and (II) NFM by (a) control, (b) BSA, and (c) EA, at a concentration of 2% (n = 3).

3.3.4. Immunoreaction Time. The optimization of the immunoreaction time was carried out by incubating the fabricated immunosensor (3PBA-BSA concentration of 10 μg mL^{-1}, immobilization time of 120 min, and substrate concentration of 1 mg mL^{-1}) with Nb-ALP at a concentration of 400 μg mL^{-1} for different times. The signal response gradually increased with the increasing time to reach a maximum and then to a platform at the time of 40 min (Figure 4d), indicating that there was no available free nanobody to match with the immobilized 3PBA-BSA after that time.

3.3.5. Substrate Concentration. Finally, the concentration of the substrate is another critical factor affecting the enzyme-catalyzed reaction.[26] With the other parameters fixed, the current response increased continuously with the concentration of 1-NP and reached the maximum value at the concentration of 1 mg mL^{-1} (Figure 4e). No further obvious increase in the response with an increase of the substrate concentration was observed afterward. So, 1 mg mL^{-1} was adopted as the ideal concentration for the best analytical performance.

3.3.6. Blocking of Remaining Active Sites of NFM. It is necessary to block any residual free active groups on the chemically modified and coating antigen-incorporated nanofiber surface to prevent any nonspecific reaction with Nb-ALP during the competition step. Incomplete blockage of the sites could affect the accuracy of the immunosensor. In some cases, the type and concentration of blocking reagents can have a large effect on assay performance. Two blocking reagents, bovine serum albumin (BSA) and ethanolamine (EA), with a concentration of 2% (w/v) were assayed. Samples of 5 mm of Ny-CA NFM and Ny-CA CM discs were incubated with the blocking solutions for 12 h at 4 °C, respectively. After washing with PBS, 100 μL Nb-ALP at a concentration of 400 μg mL^{-1} was added onto the discs for 2 h at room temperature. Consequently, the discs were washed several times with a Vortex mixer in PBS to remove unbonded Nb-ALP. The efficiency of the blocking process was evaluated by colorimetry based on the colorimetric analysis of the ALP enzyme activity using a *p*-nitrophenyl phosphate (*p*NPP) substrate. The control samples were incubated with no blocking solutions (only PBS). As shown in Figure 4F, in the case of the activated CA-Ny-CM, both reagent solutions showed the ability for full blocking of the active groups on the surface of the membranes. On the other hand, the use of BSA resulted in insufficient blocking for the active groups on the surface of the activated

https://dx.doi.org/10.1021/acsami.9b16193
ACS Appl. Mater. Interfaces 2020, 12, 6159−6168

CA-Ny NFM, while EA observed total blockage of the active sites of the nanofibrous membranes. The microporosity of the nanofibrous membranes might have restricted BSA from penetrating into the membranes since the BSA molecular size (66.5 kDa) is quite large, almost four times larger than the nanobody molecular size (about 15 Da).[43,44]

3.4. Detection of 3-Phenoxybenzoic Acid. With the optimization of the different factors, the analytical performance of the fabricated nanosensor for 3-PBA detection was investigated based on a competition between the free and immobilized 3-PBA to bind with the nanobody in the solution followed by measuring ALP-impeded-Nb activity electrochemically using the 1-NP substrate. Figure 5A shows the DPV

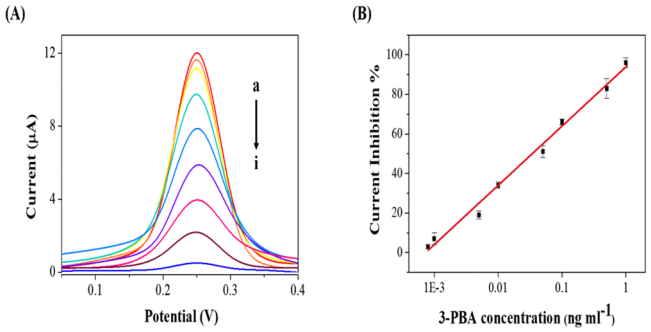

Figure 5. (A) Electrocatalytic current responses of the assembled nanobody-based electrochemical sensor for the detection of different concentrations of 3-PBA: 0 ng mL^{-1} (a), 0.0008 ng mL^{-1} (b), 0.001 ng mL^{-1} (c), 0.005 ng mL^{-1} (d), 0.01 ng mL^{-1} (e), 0.05 ng mL^{-1} (f), 0.1 ng mL^{-1} (g), 0.5 ng mL^{-1} (h), and 1 ng mL^{-1} (i). (B) Calibration curve of the immunosensor for the detection of different concentrations of 3-PBA (n = 3).

responses of the assembled nanosensor at different 3-PBA concentrations; it was obvious that the current decreased as 3-PBA concentration increased. As illustrated in Figure 5B, the current responses exhibited a linear decrease with the logarithm of the 3-PBA concentration from 0.0008 to 1 ng mL^{-1} and could be fitted into a linear regression equation: $I\%$ = 12.925 log c/ng mL^{-1} + 93.235 (R^2 = 0.9913). The developed immunosensor demonstrated a high sensitivity toward 3-PBA with a limit of detection (LOD) at 0.64 pg mL^{-1} (LOD = 3Sb/m, where Sb is the standard deviation of the blank and m is the slope of the calibration plot.). When comparing the assembled electrochemical immunosensor to other 3-PBA detection methods (Table 1), the assembled nanobody-based sensor observed a good behavior in terms of LOD; the ultrahigh sensitivity of the nanosensor could be attributed to the integration of the different technologies, including the microporous nanofibrous membranes enhancing the accessibility of the nanobody to the recognition sites and accelerating the electron transfer, consequently improving the sensing surface and the utilization of the nanobodies with their merits as an alternative to the traditional antibodies, allowing detection of the 3-PBA with high sensitivity.

3.5. Specificity, Reusability, and Stability of the Immunosensor. The ability of a sensor to specifically detect the desired target in samples containing different analogs and other molecules is considered as one of the most important challenges in the sensing technology field. The selectivity of the assembled immunosensor was investigated by examining 0.1 ng mL^{-1} of two 3-PBA analogues (3-phenoxybeneyl aldehyde and 3-phenoxybenzyl alcohol) and three pyrethroids

Table 1. Comparison of the Detection Limits of 3-PBA of the Developed Nanosensor with Other Previously Published Researches

no.	method of detection	LOD (ng mL^{-1})	ref
1	polyclonal antibodies/enzyme-linked immunosorbent assay	0.43	13
2	Mn-doped ZnS quantum dots (QDs)/optical sensor	25	25
3	colloidal gold/monoclonal antibodies/lateral-flow immunoassay	130	27
4	HPLC-UV	130	45
5	antibody fragments/Au electrode/electrochemical (EIS)	2.4	46
6	bacteriophage-assisted sandwich immunoassay/11-mercaptoundecanoic−Au electrode/electrochemical (EIS)	740	47
7	Nb-ALP/sensitive direct competitive fluorescence enzyme immunoassay (dc-FEIA)	0.011	34
8	Nb-ALP/Ny NFM-SPE/electrochemical (DPV)	0.00064	this study

(permethrin, cypermethrin, and deltamethrin) pesticides. The cross-reactivity (CR %) was studied by determining the residual current response after the competitions between each molecule and immobilized 3PBA-BSA to bind with the nanobodies. It was in terms of 3-PBA-equivalent concentration and expressed as a percentage of 3-PBA response.[9,48] As seen in Table 2, the assembled nanosensor presented a very high specificity to 3-PBA. Whereas, the different tested materials did not exhibit cross-reactivity, except 3-phenoxybeneyl aldehyde, which showed a low cross-reactivity (12.9%). This compound can rapidly convert to 3-PBA in the human body.[49]

The reusability of the sensors could be useful for minimizing the cost of the medical screening tests and reducing medical wastes. The assembled immunosensor was regenerated by dipping in a 0.1 M glycine hydrochloric acid buffer at a pH value of 2.8 for 5 min after detection of 0.1 ng mL^{-1} of 3-PBA. The assembled immunosensor demonstrated good reusability by maintaining more than 90% of its initial activity in the second cycle and about 66% after three assay runs (Figure S3). The activity loss may be due to denaturation of the bovine serum albumin or destruction of Ny NFM with repeating regeneration in an acidic glycine buffer.[50]

The immunosensor was stored at 4 °C, and its activity was evaluated every week to study the stability. The immunosensor showed good stability by maintaining more than 90% of its original activity after 5 weeks.

3.6. Applicability of the Immunosensor. In order to investigate the practicality and feasibility of the assembled nanosensor in the detection of trace amounts of 3-BPA in real samples, human urine samples were spiked with known concentrations of 3-BPA ranging from 0.01 to 0.5 ng mL^{-1}. Preceding the spiking process, the urine samples were verified by LC−MS to be free of 3-BPA. The spiked urine samples were diluted 10 times with PBS without any further treatments and then were analyzed by the immunosensor in a blind fashion. Each concentration was tested in triplicate. As illustrated in Table S1, the recovery rate was from 94.8% to about 102%, and the relative standard deviation (RSD%) was about 4.7%. The abovementioned results prove the applicability, accuracy, and reproducibility of the assembled nanosensor for fast 3-PBA detection in the human urine at

https://dx.doi.org/10.1021/acsami.9b16193
ACS Appl. Mater. Interfaces 2020, 12, 6159−6168

Table 2. Cross-Reactivity of the Developed Immunosensor for 3-PBA Analogues and Pyrethroid Pesticides at 0.1 ng mL^{-1}

compound	3-phenoxybeneyl aldehyde	3-phenoxybenzyl alcohol	permethrin	cypermethrin	deltamethrin
CR %	12.9	0	0	0	0

an extremely lower concentration without precleaning of the samples.

4. CONCLUSIONS

An ultrasensitive, disposable, and rapid detection immunosensor for monitoring human exposure to pyrethroid pesticides was successfully developed by coupling a nanobody Nb-ALP to surfaces of the nanofibers in microporous nanofibrous membranes. The developed nanosensor exhibited very attractive analytical performance with a competitive detection limit of 0.64 pg mL^{-1}. The fabricated immunosensors possess the advantage of easy use, low-cost assay, reusability, and fast analysis where the sample analysis could be accomplished in less than 45 min. The new immunosensor could be a promising alternative tool to the traditional methods for point-of-care detection of 3-PBA.

■ ASSOCIATED CONTENT

Supporting Information

The Supporting Information is available free of charge at https://pubs.acs.org/doi/10.1021/acsami.9b16193.

(Figure S1) FTIR of Ny-CA NFM with different initial CA concentrations (a) 3%, (b) 4%, (c). 6%, and (d) 8%; (Figure S2) contact angles of Ny NFM before and after grafting with citric acid; (Figure S3) reusability of the fabricated immunosensor after regeneration by dipping the immunosensor into a 0.1 M glycine hydrochloric acid buffer (pH 2.8) for 5 min after 3-PBA detection at concentration of 0.1 ng mL^{-1}; (Table S1) recoveries of 3-PBA from spiked human urine samples determined by the immunosensor (PDF)

■ AUTHOR INFORMATION

Corresponding Authors

Ahmed Y. El-Moghazy − *Department of Biological and Agricultural Engineering, University of California, Davis 95616, USA; Polymeric Materials Research Department, Advanced Technology and New Materials Research Institute, City of Scientific Research and Technological Applications (SRTA-City), New Borg El-Arab City, Egypt;* orcid.org/0000-0002-5743-7305; Email: aelmoghazy@ucdavis.edu

Gang Sun − *Department of Biological and Agricultural Engineering, University of California, Davis 95616, USA;* orcid.org/0000-0002-6608-9971; Email: gysun@ucdavis.edu

Authors

Jingqian Huo − *Department of Entomology and Nematology and UCD Comprehensive Cancer Center, University of California, Davis, California 95616, United States; College of Plant Protection, Agricultural University of Hebei, Baoding 071001, P. R. China*

Noha Amaly − *Department of Biological and Agricultural Engineering, University of California, Davis 95616, USA; Polymeric Materials Research Department, Advanced Technology and New Materials Research Institute, City of Scientific Research and Technological Applications (SRTA-City), New Borg El-Arab City, Egypt*

Natalia Vasylieva − *Department of Entomology and Nematology and UCD Comprehensive Cancer Center, University of California, Davis, California 95616, United States*

Bruce D. Hammock − *Department of Entomology and Nematology and UCD Comprehensive Cancer Center, University of California, Davis, California 95616, United States;* orcid.org/0000-0003-1408-8317

Complete contact information is available at: https://pubs.acs.org/10.1021/acsami.9b16193

Notes

The authors declare no competing financial interest.

■ ACKNOWLEDGMENTS

The authors thank the support of the National Institute of Environmental Health Science Superfund Research Program (P42ES004699), the National Academy of Sciences (NAS, Subaward no. 2000009144), and the National Nature Science Foundation of China (no. 31471786). The article is derived from the subject data funded in part by NAS and USAID, and that any opinions, findings, conclusions, or recommendations expressed in such article are those of the authors alone and do not necessarily reflect the views of USAID or NAS.

■ REFERENCES

(1) Hu, M.-X.; Li, J.-N.; Guo, Q.; Zhu, Y.-Q.; Niu, H.-M. Probiotics Biofilm-Integrated Electrospun Nanofiber Membranes: A New Starter Culture for Fermented Milk Production. *J. Agric. Food Chem.* **2019**, *67*, 3198−3208.

(2) Li, X.; Wang, C.; Huang, X.; Zhang, T.; Wang, X.; Min, M.; Wang, L.; Huang, H.; Hsiao, B. S. Anionic Surfactant-Triggered Steiner Geometrical Poly(Vinylidene Fluoride) Nanofiber/Nanonet Air Filter for Efficient Particulate Matter Removal. *ACS Appl. Mater. Interfaces* **2018**, *10*, 42891−42904.

(3) Amaly, N.; Si, Y.; Chen, Y.; El-Moghazy, A. Y.; Zhao, C.; Zhang, R.; Sun, G. Reusable Anionic Sulfonate Functionalized Nanofibrous Membranes for Cellulase Enzyme Adsorption and Separation. *Colloids Surf., B* **2018**, *170*, 588−595.

(4) Ramadan, M.; Abdellah, A. M.; Mohamed, S. G.; Allam, N. K. 3D Interconnected Binder-Free Electrospun MnO@C Nanofibers for Supercapacitor Devices. *Sci. Rep.* **2018**, *8*, 7988.

(5) Liu, X.; Marlow, M. N.; Cooper, S. J.; Song, B.; Chen, X.; Brandon, N. P.; Wu, B. Flexible All-Fiber Electrospun Supercapacitor. *J. Power Sources* **2018**, *384*, 264−269.

(6) Awada, H.; Al Samad, A.; Laurencin, D.; Gilbert, R.; Dumail, X.; El Jundi, A.; Bethry, A.; Pomrenke, R.; Johnson, C.; Lemaire, L.; et al. Controlled Anchoring of Iron Oxide Nanoparticles on Polymeric Nanofibers: Easy Access to Core@Shell Organic−Inorganic Nanocomposites for Magneto-Scaffolds. *ACS Appl. Mater. Interfaces* **2019**, *11*, 9519−9529.

(7) Mao, Z.; Li, J.; Huang, W.; Jiang, H.; Zimba, B. L.; Chen, L.; Wan, J.; Wu, Q. Preparation of Poly(Lactic Acid)/Graphene Oxide Nanofiber Membranes with Different Structures by Electrospinning for Drug Delivery. *RSC Adv.* **2018**, *8*, 16619−16625.

(8) Wang, Y.; Cui, W.; Zhao, X.; Wen, S.; Sun, Y.; Han, J.; Zhang, H. Bone Remodeling-Inspired Dual Delivery Electrospun Nanofibers for Promoting Bone Regeneration. *Nanoscale* **2019**, *11*, 60−71.

(9) El-Moghazy, A. Y.; Zhao, C.; Istamboulie, G.; Amaly, N.; Si, Y.; Noguer, T.; Sun, G. Ultrasensitive Label-Free Electrochemical Immunosensor Based on PVA-Co-PE Nanofibrous Membrane for

the Detection of Chloramphenicol Residues in Milk. *Biosens. Bioelectron.* **2018**, *117*, 838−844.
(10) El-Moghazy, A. Y.; Soliman, E. A.; Ibrahim, H. Z.; Marty, J.-L.; Istamboulie, G.; Noguer, T. Biosensor Based on Electrospun Blended Chitosan-Poly (Vinyl Alcohol) Nanofibrous Enzymatically Sensitized Membranes for Pirimiphos-Methyl Detection in Olive Oil. *Talanta* **2016**, *155*, 258−264.
(11) Dong, C.; Wang, H.; Zhang, Z.; Zhang, T.; Liu, B. Carboxybetaine Methacrylate Oligomer Modified Nylon for Circulating Tumor Cells Capture. *J. Colloid Interface Sci.* **2014**, *432*, 135−143.
(12) Edmondson, S.; Osborne, V. L.; Huck, W. T. S. Polymer Brushes via Surface-Initiated Polymerizations. *Chem. Soc. Rev* **2004**, *33*, 14−22.
(13) McCoy, M. R.; Yang, Z.; Fu, X.; Ahn, K. C.; Gee, S. J.; Bom, D. C.; Zhong, P.; Chang, D.; Hammock, B. D. Monitoring of Total Type II Pyrethroid Pesticides in Citrus Oils and Water by Converting to a Common Product 3-Phenoxybenzoic Acid. *J. Agric. Food Chem.* **2012**, *60*, 5065−5070.
(14) Casida, J. E.; Quistad, G. B. Golden Age of Insecticide Research: Past, Present, or Future? *Annu. Rev. Entomol.* **1998**, *43*, 1−16.
(15) Shafer, T. J.; Meyer, D. A.; Crofton, K. M. Developmental Neurotoxicity of Pyrethroid Insecticides: Critical Review and Future Research Needs. *Environ. Health Perspect.* **2005**, *113*, 123−136.
(16) Yuan, C.; Wang, C.; Gao, S.-Q.; Kong, T.-T.; Chen, L.; Li, X.-F.; Song, L.; Wang, Y.-B. Effects of Permethrin, Cypermethrin and 3-Phenoxybenzoic Acid on Rat Sperm Motility in Vitro Evaluated with Computer-Assisted Sperm Analysis. *Toxicol. In Vitro* **2010**, *24*, 382−386.
(17) Sun, H.; Chen, W.; Xu, X.; Ding, Z.; Chen, X.; Wang, X. Pyrethroid and Their Metabolite, 3-Phenoxybenzoic Acid Showed Similar (Anti)Estrogenic Activity in Human and Rat Estrogen Receptor α-Mediated Reporter Gene Assays. *Environ. Toxicol. Pharmacol.* **2014**, *37*, 371−377.
(18) Jin-Ok, C.; Jitsunari, F.; Asakawa, F.; Suna, S.; Manabe, Y.; Takeda, N. Study on Biological Monitoring of Fenpropathrin Exposure in Application by Utilizing Urinary 3-Phenoxybenzoic Acid Level. *Environ. Health Prev. Med.* **1998**, *2*, 145−150.
(19) Fortes, C.; Mastroeni, S.; Pilla, M. A.; Antonelli, G.; Lunghini, L.; Aprea, C. The Relation between Dietary Habits and Urinary Levels of 3-Phenoxybenzoic Acid, a Pyrethroid Metabolite. *Food Chem. Toxicol.* **2013**, *52*, 91−96.
(20) Trunnelle, K. J.; Bennett, D. H.; Ahn, K. C.; Schenker, M. B.; Tancredi, D. J.; Gee, S. J.; Stoecklin-Marois, M. T.; Hammock, B. D. Concentrations of the Urinary Pyrethroid Metabolite 3-Phenoxybenzoic Acid in Farm Worker Families in the MICASA Study. *Environ. Res.* **2014**, *131*, 153−159.
(21) Liu, F.; Chi, Y.; Wu, S.; Jia, D.; Yao, K. Simultaneous Degradation of Cypermethrin and Its Metabolite, 3-Phenoxybenzoic Acid, by the Cooperation of *Bacillus Licheniformis* B-1 and *Sphingomonas* Sp. SC-1. *J. Agric. Food Chem.* **2014**, *62*, 8256−8262.
(22) Chung, S. W. C.; Lam, C. H. Development and Validation of a Method for Determination of Residues of 15 Pyrethroids and Two Metabolites of Dithiocarbamates in Foods by Ultra-Performance Liquid Chromatography−Tandem Mass Spectrometry. *Anal. Bioanal. Chem.* **2012**, *403*, 885−896.
(23) Ding, Y.; White, C. A.; Muralidhara, S.; Bruckner, J. V.; Bartlett, M. G. Determination of Deltamethrin and Its Metabolite 3-Phenoxybenzoic Acid in Male Rat Plasma by High-Performance Liquid Chromatography. *J. Chromatogr. B* **2004**, *810*, 221−227.
(24) Mudiam, M. K. R.; Jain, R.; Singh, A.; Khan, H. A.; Parmar, D. Development of Ultrasound-Assisted Dispersive Liquid−Liquid Microextraction−Large Volume Injection−Gas Chromatography−Tandem Mass Spectrometry Method for Determination of Pyrethroid Metabolites in Brain of Cypermethrin-Treated Rats. *Forensic Toxicol.* **2014**, *32*, 19−29.
(25) Pandey, V.; Chauhan, A.; Pandey, G.; Mudiam, M. K. R. Optical Sensing of 3-Phenoxybenzoic Acid as a Pyrethroid Pesticides Exposure Marker by Surface Imprinting Polymer Capped on Manganese-Doped Zinc Sulfide Quantum Dots. *Anal. Chem. Res.* **2015**, *5*, 21−27.
(26) Thiphom, S.; Prapamontol, T.; Chantara, S.; Mangklabruks, A.; Suphavilai, C.; Ahn, K. C.; Gee, S. J.; Hammock, B. D. Determination of the Pyrethroid Insecticide Metabolite 3-PBA in Plasma and Urine Samples from Farmer and Consumer Groups in Northern Thailand. *J. Environ. Sci. Health, Part B* **2014**, *49*, 15−22.
(27) Liu, Y.; Wu, A.; Hu, J.; Lin, M.; Wen, M.; Zhang, X.; Xu, C.; Hu, X.; Zhong, J.; Jiao, L.; et al. Detection of 3-Phenoxybenzoic Acid in River Water with a Colloidal Gold-Based Lateral Flow Immunoassay. *Anal. Biochem.* **2015**, *483*, 7−11.
(28) Felix, F. S.; Angnes, L. Electrochemical Immunosensors − A Powerful Tool for Analytical Applications. *Biosens. Bioelectron.* **2018**, *102*, 470−478.
(29) Rasmussen, S. G. F.; Choi, H.-J.; Fung, J. J.; Pardon, E.; Casarosa, P.; Chae, P. S.; Devree, B. T.; Rosenbaum, D. M.; Thian, F. S.; Kobilka, T. S.; et al. Structure of a Nanobody-Stabilized Active State of the B2 Adrenoceptor. *Nature* **2011**, *469*, 175−180.
(30) Muyldermans, S. Nanobodies: Natural Single-Domain Antibodies. *Annu. Rev. Biochem.* **2013**, *82*, 775−797.
(31) Leduc, C.; Si, S.; Gautier, J.; Soto-Ribeiro, M.; Wehrle-Haller, B.; Gautreau, A.; Giannone, G.; Cognet, L.; Lounis, B. A Highly Specific Gold Nanoprobe for Live-Cell Single-Molecule Imaging. *Nano Lett.* **2013**, *13*, 1489−1494.
(32) Cairns, T. L.; Foster, H. D.; Larchar, A. W.; Schneider, A. K.; Schreiber, R. S. Preparation and Properties of N-Methylol, N-AlkoxymEthyl and N-Alkylthiomethyl Polyamides. *J. Am. Chem. Soc* **1949**, *71*, 651−655.
(33) Shieh, J.-J.; Huang, R. Y. M. Preparation of N-Methylol Nylon-6 Membranes for Pervaporation of Ethanol-Water Mixtures. *J. Appl. Polym. Sci.* **1997**, *64*, 855−863.
(34) Huo, J.; Li, Z.; Wan, D.; Li, D.; Qi, M.; Barnych, B.; Vasylieva, N.; Zhang, J.; Hammock, B. D. Development of a Highly Sensitive Direct Competitive Fluorescence Enzyme Immunoassay Based on a Nanobody−Alkaline Phosphatase Fusion Protein for Detection of 3-Phenoxybenzoic Acid in Urine. *J. Agric. Food Chem.* **2018**, *66*, 11284−11290.
(35) Shan, G.; Huang, H.; Stoutamire, D. W.; Gee, S. J.; Leng, G.; Hammock, B. D. A Sensitive Class Specific Immunoassay for the Detection of Pyrethroid Metabolites in Human Urine. *Chem. Res. Toxicol.* **2004**, *17*, 218−225.
(36) Fu, Q.; Wang, X.; Si, Y.; Liu, L.; Yu, J.; Ding, B. Scalable Fabrication of Electrospun Nanofibrous Membranes Functionalized with Citric Acid for High-Performance Protein Adsorption. *ACS Appl. Mater. Interfaces* **2016**, *8*, 11819−11829.
(37) Cerroni, B.; Cicconi, R.; Oddo, L.; Scimeca, M.; Bonfiglio, R.; Bernardini, R.; Palmieri, G.; Domenici, F.; Bonanno, E.; Mattei, M.; et al. In Vivo Biological Fate of Poly(Vinylalcohol) Microbubbles in Mice. *Heliyon* **2018**, *4*, No. e00770.
(38) Eckhard, K.; Shin, H.; Mizaikoff, B.; Schuhmann, W.; Kranz, C. Alternating Current (AC) Impedance Imaging with Combined Atomic Force Scanning Electrochemical Microscopy (AFM-SECM). *Electrochem. commun.* **2007**, *9*, 1311−1315.
(39) Liu, X.; Li, Q.; Chen, L.; Zhou, J.; Liu, M.; Shen, Y. One-Step Immobilization Antibodies Using Ferrocene-Containing Thiol Aromatic Aldehyde for the Fabrication of a Label-Free Electrochemical Immunosensor. *RSC Adv.* **2016**, *6*, 114019−114023.
(40) Hammond, J. L.; Formisano, N.; Estrela, P.; Carrara, S.; Tkac, J. Electrochemical Biosensors and Nanobiosensors. *Essays Biochem.* **2016**, *60*, 69−80.
(41) Li, Y.; Afrasiabi, R.; Fathi, F.; Wang, N.; Xiang, C.; Love, R.; She, Z.; Kraatz, H.-B. Impedance Based Detection of Pathogenic *E. coli* O157: H7 Using a Ferrocene-Antimicrobial Peptide Modified Biosensor. *Biosens. Bioelectron.* **2014**, *58*, 193−199.
(42) Santaclara, F. J.; Pérez-Martín, R. I.; Sotelo, C. G. Developed of a Method for the Genetic Identification of Ling Species (Genypterus Spp.) in Seafood Products by FINS Methodology. *Food Chem.* **2014**, *143*, 22−26.

https://dx.doi.org/10.1021/acsami.9b16193
ACS Appl. Mater. Interfaces 2020, 12, 6159−6168

(43) Wang, J.; Mukhtar, H.; Ma, L.; Pang, Q.; Wang, X. VHH Antibodies: Reagents for Mycotoxin Detection in Food Products. *Sensors* **2018**, *18*, 485.
(44) Ren, X.; Yan, J.; Wu, D.; Wei, Q.; Wan, Y. Nanobody-Based Apolipoprotein e Immunosensor for Point-of-Care Testing. *ACS Sensors* **2017**, *2*, 1267−1271.
(45) Li, J.; Lin, D.; Ji, R.; Yao, K.; Deng, W.-Q.; Yuan, H.; Wu, Q.; Jia, Q.; Luo, P.; Zhou, K.; et al. Simultaneous Determination of β-Cypermethrin and Its Metabolite 3-Phenoxybenzoic Acid in Microbial Degradation Systems by HPLC-UV. *J. Chromatogr. Sci.* **2016**, *54*, 1584−1592.
(46) Pali, M.; Suni, I. I. Impedance Detection of 3-Phenoxybenzoic Acid Comparing Wholes Antibodies and Antibody Fragments for Biomolecular Recognition. *Electroanalysis* **2018**, *30*, 2899−2907.
(47) Pali, M.; Bever, C. R. S.; Vasylieva, N.; Hammock, B. D.; Suni, I. I. Impedance Detection of 3-Phenoxybenzoic Acid with a Noncompetitive Two-Site Phage Anti-Immunocomplex Assay. *Electroanalysis* **2018**, *30*, 2653−2659.
(48) Gaudin, V.; Maris, P. Development of a Biosensor- Based Immunoassay for Screening of Chloramphenicol Residues in Milk. *Food Agric. Immunol.* **2010**, 77−86.
(49) Kim, H. J.; Ahn, K. C.; González-Techera, A.; González-Sapienza, G. G.; Gee, S. J.; Hammock, B. D. Magnetic Bead-Based Phage Anti-Immunocomplex Assay (PHAIA) for the Detection of the Urinary Biomarker 3-Phenoxybenzoic Acid to Assess Human Exposure to Pyrethroid Insecticides. *Anal Biochem.* **2009**, *386*, 45−52.
(50) Qiao, L.; Wang, X.; Sun, X. A Novel Label-Free Amperometric Immunosensor Based on Graphene Sheets-Methylene Blue Nanocomposite/Gold Nanoparticles. *Int. J. Electrochem. Sci.* **2014**, *9*, 1399−1414.

https://dx.doi.org/10.1021/acsami.9b16193
ACS Appl. Mater. Interfaces 2020, 12, 6159−6168